nature COMMUNICATIONS

ARTICLE

Received 9 Jun 2014 | Accepted 5 Nov 2014 | Published 8 Dec 2014

DOI: 10.1038/ncomms6761

Intra-unit-cell nematic charge order in the titanium-oxypnictide family of superconductors

Benjamin A. Frandsen[1,*], Emil S. Bozin[2,*], Hefei Hu[2,†], Yimei Zhu[2], Yasumasa Nozaki[3], Hiroshi Kageyama[3], Yasutomo J. Uemura[1], Wei-Guo Yin[2] & Simon J.L. Billinge[2,4]

Understanding the role played by broken-symmetry states such as charge, spin and orbital orders in the mechanism of emergent properties, such as high-temperature superconductivity, is a major current topic in materials research. That the order may be within one unit cell, such as nematic, was only recently considered theoretically, but its observation in the iron-pnictide and doped cuprate superconductors places it at the forefront of current research. Here, we show that the recently discovered $BaTi_2Sb_2O$ superconductor and its parent compound $BaTi_2As_2O$ form a symmetry-breaking nematic ground state that can be naturally explained as an intra-unit-cell nematic charge order with *d*-wave symmetry, pointing to the ubiquity of the phenomenon. These findings, together with the key structural features in these materials being intermediate between the cuprate and iron-pnictide high-temperature superconducting materials, render the titanium oxypnictides an important new material system to understand the nature of nematic order and its relationship to superconductivity.

---

[1] Department of Physics, Columbia University, New York, New York 10027, USA. [2] Condensed Matter Physics and Materials Science Department, Brookhaven National Laboratory, Upton, New York 11973, USA. [3] Department of Energy and Hydrocarbon Chemistry, Graduate School of Engineering, Kyoto University, Nishikyo, Kyoto 615-8510, Japan. [4] Department of Applied Physics and Applied Mathematics, Columbia University, New York, New York 10027, USA. * These authors contributed equally to this work. † Present address: Intel Corporation, Folsom, California 95630, USA. Correspondence and requests for materials should be addressed to S.J.L.B. (email: sb2896@columbia.edu).

Rather than being an anomalous side effect in one or two cuprate systems, broken-symmetry states are now thought to be widespread in strongly correlated electron systems and other complex materials. Extensive study of the manganites[1,2], cuprates[3,4], iron pnictides[5] and a variety of other systems has made it increasingly evident that local and global symmetry breaking in the charge, orbital, lattice and spin degrees of freedom are associated with the appearance of emergent phenomena, such as colossal magnetoresistance and high-temperature superconductivity (HTSC), but the exact relationship is not understood. Historically, the study of such broken-symmetry states has been very challenging. Taking the cuprates as an example, 8 years elapsed from the initial discovery of superconductivity to the first observation of symmetry-broken charge order (stripes) in one system[6], another 7 years passed before hints were found in others[7,8] and only within the last 3 years has charge order begun to emerge as a possibly ubiquitous feature of the cuprates[9,10].

Several possibilities arise when considering the symmetries that can be broken by these states. Most charge-/spin-density waves (C/SDWs) break the translational symmetry of the lattice, folding the Brillouin zone and resulting in superlattice diffraction peaks. On the other hand, orbital ordering, where charge transfers between orbitals centred at the same site, can break the metric rotational symmetry without lowering the translational symmetry. Examples are charge-nematic[11] and loop-current[12,13] orders in the doped cuprates. In this context, nematic order is defined as one that breaks the rotational point group symmetry while preserving the lattice translational symmetry. The fact that nematic symmetry-broken states have recently been discovered experimentally in both the cuprate[11] and iron-based[14] superconductors raises the importance and relevance of this observation to HTSC. It is, therefore, critically important to understand the role and ubiquity of symmetry breaking, including intra-unit-cell nematicity, to the superconducting phenomenon.

Standard theoretical treatments of HTSC, such as the effective single-band t–J model, have typically ignored the possibility of intra-unit-cell orders[15]. When multiple atoms per unit cell are explicitly included in the theory, qualitatively different ground-state solutions may be found[16], underscoring the subtlety and importance of accounting correctly for this phenomenon. Hence, finding related but distinct systems that exhibit this phenomenon is expected to shed new light on this critical question.

Very recently, superconductivity was discovered[17–19] in titanium-oxypnictide compounds, such as $A\mathrm{Ti_2}Pn_2\mathrm{O}$ ($A = \mathrm{Na_2}$, Ba, (SrF)$_2$, (SmO)$_2$; $Pn =$ As, Sb, Bi), which are close structural and chemical cousins to the cuprates and iron-pnictides[20–24]. In particular, in isovalent BaTi$_2$(Sb$_{1-x}$Bi$_x$)$_2$O and aliovalent Ba$_{1-x}$Na$_x$Ti$_2$Sb$_2$O (ref. 25), muon spin rotation and heat capacity measurements point to fully-gapped s-wave superconductivity[26–28]. Interestingly, a number of compounds in this family also show strong anomalies in resistivity and/or magnetic susceptibility that are thought to be signatures of symmetry-breaking charge- or spin-ordered ground states[21,24,25,29,30], suggesting that these materials are excellent candidates for studying the interplay between broken-symmetry states and superconductivity. In light of these strong transport anomalies, it is then quite surprising that subsequent experiments have failed to uncover any direct evidence for a conventional spin- or charge-density wave ground state[26,27,31], leaving open the question of whether these materials do possess symmetry-broken ground states.

Here, we show that superconducting BaTi$_2$Sb$_2$O, and its non-superconducting parent compound BaTi$_2$As$_2$O, do indeed undergo a tetragonal-orthorhombic phase transition, corresponding to a C$_4$–C$_2$ symmetry lowering, that occurs at the temperature of the transport anomaly. On the other hand, high-sensitivity electron diffraction measurements failed to detect any superlattice peaks in the bulk at low temperature, indicating that this transition does not break translational symmetry. The low-temperature phase, therefore, constitutes a nematic state. In light of the pronounced upturn in resistivity accompanying this nematic transition, together with the absence of any ordered SDW[26], we attribute the nematicity to an intra-unit-cell charge order with d-wave symmetry by charge transfer between neighbouring Ti sites—similar to that between neighbouring oxygen sites in cuprate superconductors—and find that it naturally explains the temperature dependence of the lattice constants. These results establish this family of materials as another playground for studying symmetry-breaking electronic phases and their relationship to superconductivity.

Results

Structural and electronic properties of BaTi$_2$$Pn_2$O. The basic structural unit of BaTi$_2$$Pn_2$O is a planar square net of titanium and oxygen, in analogy with the cuprates (Fig. 1a,b), with the crucial difference that the positions of the metal and oxygen ions are switched between the structures (the complete titanate structure is shown as an inset in Fig. 2b). In Fig. 1, the square net is shown by solid lines along the nearest neighbour bonds, with dashed lines showing the net joining second neighbour ions. This second-nearest-neighbour square net connects oxygen ions in the cuprates, but metal ions in the titanate compounds and also in the iron-based superconductors (Fig. 1c). Thus, in terms of chemistry and structure, the titanate compounds bridge between the ferrous and cuprate superconductors. The Ti 3d orbitals are occupied by one electron per Ti atom, which is found to reside in a nominally 1/4-filled band formed via hybridization of the d_{xy} and $d_{y^2-z^2}/d_{x^2-z^2}$ orbitals for the Ti(1)/Ti(2) ions (defined in Fig. 1b). The local geometry of the Ti(1) site is shown in Fig. 1d and the arrangement of the d-energy levels is shown in Fig. 1e.

Furthermore, the phase diagram (Fig. 2b) is highly reminiscent of the cuprates and iron-based superconductors, with superconductivity appearing on doping and transport behaviour that is strongly suggestive of a competing electronic transition such as the formation of a CDW or SDW[21,24]. The transport is metallic at high temperature[21], with a positive resistivity slope versus temperature (Fig. 2a). However, on cooling, a pronounced upturn in the resistivity is found for all x in the solid solution BaTi$_2$As$_{1-x}$Sb$_x$O. The feature occurs at a temperature T_a that decreases monotonically from 200 K for $x = 0$ to 50 K for $x = 1$, with superconductivity appearing below ∼1 K for the antimony endmember and increasing to 5 K for BaTi$_2$Bi$_2$O (refs 19,24). Anomalies in the magnetic susceptibility and specific heat are also observed[21] at T_a.

Density functional theory (DFT) calculations for BaTi$_2$Sb$_2$O predicted an instability towards a bicollinear SDW formation[32,33] or a commensurate CDW ground state driven by an unstable phonon mode that doubles the unit cell by distorting the Ti squares and preserves the tetragonal symmetry[34]. The possibility of SDW formation in BaTi$_2$(As,Sb)$_2$O, either commensurate or incommensurate, was subsequently ruled out by muon spin relaxation and $^{121/123}$Sb nuclear resonance measurements, which show conclusively that no magnetic order develops at any temperature probed[26,27,31]. On the other hand, a conventional CDW should be evident through an associated structural distortion. However, initial electron and neutron diffraction studies on the Sb endmember[26] found no broken symmetry or any signature of superlattice formation at low temperatures, nor was a CDW gap formation observed in angle-resolved photoemission measurements of the nested Fermi surfaces

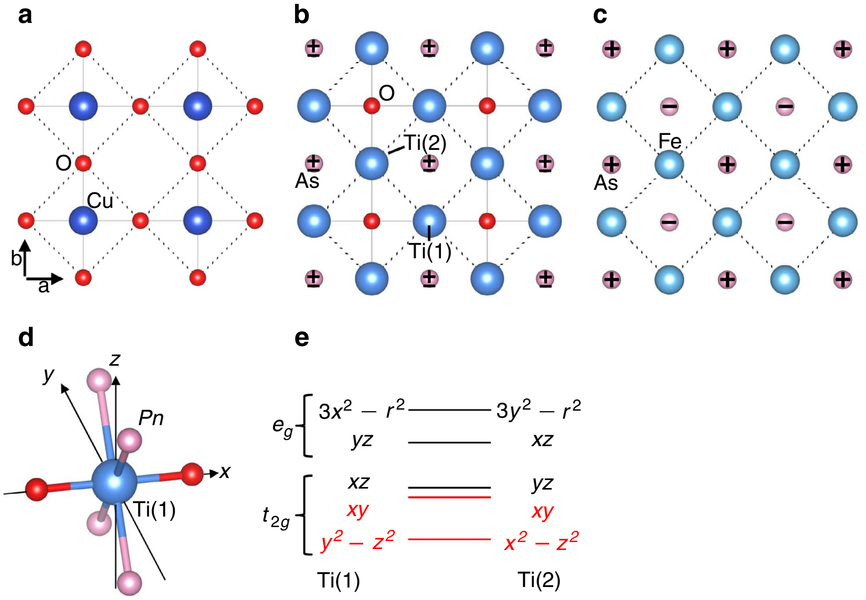

Figure 1 | Planar geometries of cuprate, titanium-oxypnictide, and iron-pnictide superconducting families. (**a**–**c**) Planar motifs in cuprates, titanium oxypnictides and iron pnictides, respectively. Solid grey lines show the metal-anion square net, and dotted black lines show the square net of second-nearest-neighbour atoms. The + and − signs in **b** and **c** denote As atoms that are above and below the plane, respectively. (**d**) TiO_2Pn_4 octahedral motif found in $BaTi_2Pn_2O$. (**e**) Schematics of the Ti 3*d*-orbital energy levels for the two distinct Ti sites labelled in **b**, Ti(1) and Ti(2). The two lowest-lying orbitals marked in red form two bands occupied by one electron per Ti.

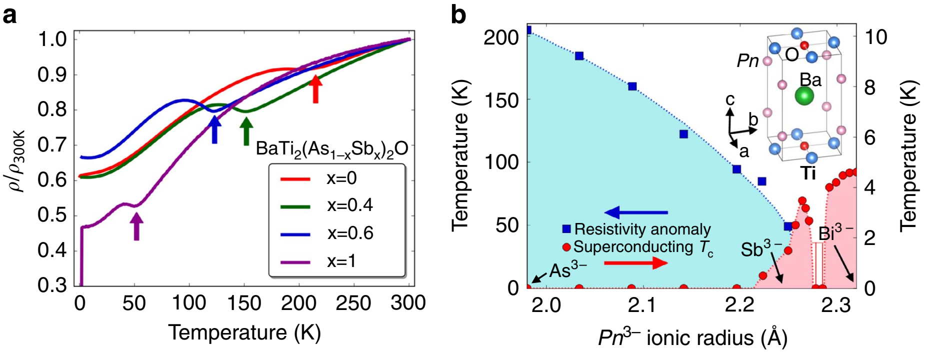

Figure 2 | Transport characteristics and phase diagram of $BaTi_2Pn_2O$ with *Pn* = As, Sb, Bi. (**a**) Electrical resistivity of $BaTi_2(As_{1-x}Sb_x)_2O$, normalized by the room temperature resistivity. Arrows indicate the anomaly discussed in the text. (**b**) Phase diagram of $BaTi_2Pn_2O$ shown as a function of Pn^{3-} ionic diameter. Broken lines are guides to the eye. The error bars accompanying the red circles arise from the instrumental low-temperature limit of 1.8 K. Inset: tetragonal crystal structure of $BaTi_2Pn_2O$.

(although a slight depression of the density of states at other momenta was found to correlate in temperature with the resistivity anomaly[35]). The possibility of an incommensurate CDW was also ruled out by $^{121/123}Sb$ nuclear resonance measurements[31].

Neutron powder diffraction measurements. In the absence of evidence for a long-range ordered CDW, we undertook a neutron diffraction and total scattering measurement on $BaTi_2Sb_2O$ with a dense set of temperature points to search for evidence for a possible short-range ordered CDW[36,37]. We also extended the investigation to the previously unstudied $BaTi_2As_2O$ endmember. Unexpectedly, we found a long-range structural phase transition at T_a. Room temperature measurements of $BaTi_2As_2O$ confirm the tetragonal *P*4/*mmm* space-group symmetry previously reported from X-ray diffraction[21]. However, on cooling through T_a, we observe a distinct splitting of the (200)/(020) and (201)/(021) Bragg peaks, representing the first observation of a symmetry lowering at the same temperature as the resistivity anomaly in $BaTi_2As_2O$. This is shown in Fig. 3, which compares the high- and low-temperature Bragg peaks in panel (a) and displays their temperature evolution in panel (b). The (200) peak at 2.02 Å begins to broaden below 200 K, coinciding with T_a, and appears to split at the lowest temperatures. Similarly, the (201) peak at 1.94 Å displays apparent splitting as the temperature is lowered. These observations demonstrate that $BaTi_2As_2O$ undergoes a long-range ordered structural phase change at T_a, lowering its symmetry from tetragonal to orthorhombic.

To investigate the structural transition in greater detail, we performed Le Bail[38] refinements at all temperatures. We used the parent *P*4/*mmm* model for $T \geq 200$ K. The simplest possible symmetry-breaking distortion mode of the parent *P*4/*mmm* structure consistent with the observed peak splitting is a mode that breaks the degeneracy of the *a*- and *b*-axes without otherwise shifting atoms within the unit cell, resulting in a space-group

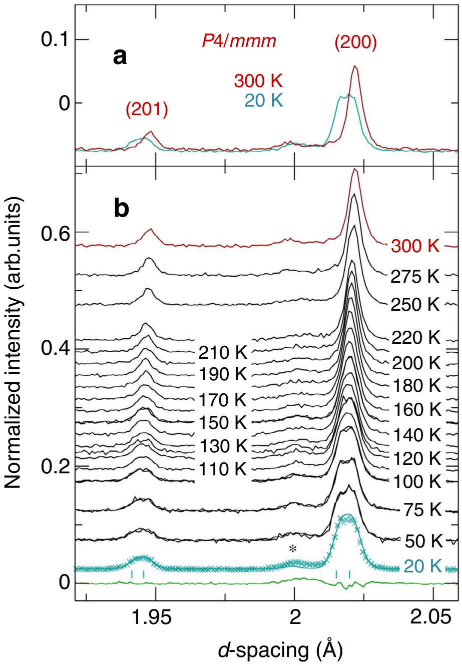

Figure 3 | Temperature evolution of $BaTi_2As_2O$ neutron diffraction pattern. (**a**) Comparison of normalized intensities of 300 K (red) and 20 K (blue) data around (200) and (201) reflections in *P4/mmm* setting. (**b**) Waterfall plot across the temperature range studied. The 20 K data (blue symbols) are shown with a fit (blue solid line) of the refined *Pmmm* model. The corresponding difference curve is shown as the green solid line below. The asterisk marks the (200)/(020) reflections of the $BaTiO_3$ impurity phase.

symmetry of *Pmmm*, which was used for $T<200$ K. We also explored other candidate orthorhombic structures with lower symmetry, but since these structures do not improve the fit quality within the resolution limitations of the current data, *Pmmm* is the most appropriate choice. We display the results of these refinements in Fig. 4. As seen in panel (b), the tetragonal *a* axis clearly splits below $T\sim200$ K, with a maximum orthorhombic splitting of ~0.01 Å. The orthorhombicity parameter $\eta=2\times(a-b)/(a+b)$ is shown in the inset of panel (a), indicating a maximum orthorhombicity of $\sim0.22\%$. Panel (a) also displays the temperature dependence of the *c* axis parameter, which exhibits an upturn below the structural transition deviating from the linear thermal contraction trend seen for $T>200$ K. This same type of *c* axis response also accompanies long-range ordered stripe formation in the nickelates[36]. Additional details regarding Rietveld refinement of $BaTi_2As_2O$ can be found in Supplementary Note 1. The superconducting $BaTi_2Sb_2O$ shows qualitatively the same behaviour, albeit with an amplitude decreased by a factor of ~5, with an orthorhombic splitting (0.05%) and a small but observable *c* axis upturn appearing on cooling through $T_a=50$ K. The undistorted *P4/mmm* model can be used with moderate success at all temperatures, but the *Pmmm* model yields a better fit below 50 K (see Supplementary Note 2). Pair distribution function analysis is consistent with these observations for both compounds and can be found in Supplementary Note 3.

These results offer compelling evidence that the observed structural response is intimately related to the transport anomaly and may be driven by a broken symmetry of the electronic system forming at that temperature. The small distortion amplitude in $BaTi_2Sb_2O$ explains why this long-range structural phase change escaped notice in previous neutron diffraction measurements[26].

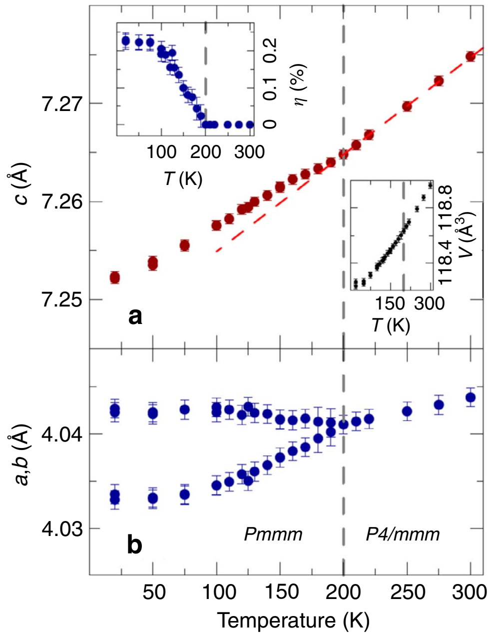

Figure 4 | Temperature evolution of $BaTi_2As_2O$ structural parameters. (**a**) Lattice parameter *c* (red). (**b**) Lattice parameters *a*, *b* (blue). Insets: orthorhombicity $\eta=2\times(a-b)/(a+b)$ (left) and unit cell volume (right). Vertical dashed grey line indicates transition temperature. Dashed red line is a guide for the eyes. Error bars represent the estimated standard deviation of the corresponding refined parameter.

Electron diffraction measurements. Since CDW formation is implicated, we made a special effort to search for the appearance of weak superlattice peaks associated with a finite CDW wavevector in electron diffraction (ED) patterns below T_a. The original study on the antimony endmember failed to observe superlattice peaks[26]. Here, we concentrated on the arsenic endmember where the structural distortion is five times larger, and the ED patterns were heavily overexposed to search for any weak response at intensities close to background. Despite these efforts, the ED patterns taken along the [001] and [011] directions revealed no superlattice peaks in the bulk at low temperature, as shown in Fig. 5. However, in a very small fraction of the sample in the immediate vicinity of grain boundaries, weak superlattice peaks with $\mathbf{Q}=(1/2, 0, 0)$ are observed at low temperature. This non-bulk behaviour is explored further in Supplementary Note 4.

Discussion

A picture emerges of a C_4–C_2 symmetry breaking occurring with an accompanying strong upturn in resistivity, but with no corresponding CDW superlattice peaks appearing. The resistivity upturn is larger than would be expected as a passive response of the electronic system to the structural transition, borne out by a standard DFT calculation with the observed orthorhombicity parameter $\eta=0.22\%$, which showed that merely 0.0003 electrons are transferred from Ti(1) to Ti(2). Therefore, in common with earlier discussion[18,21], we propose that the structural transition is a response to an instability of the electronic system. The earlier muon spin relaxation results[26,27], together with the ED measurements, allow us to rule out the existing proposals of SDW formation[32,33] or a phonon-driven CDW[34]. Instead, an intra-unit-cell charge-nematic electronic symmetry breaking is implicated, similar to that proposed for doped cuprates[39].

In the current case, a charge redistribution between the on-site orbital states at the Fermi level, $d_{x^2-z^2}/d_{y^2-z^2}$ to d_{xy}, does not

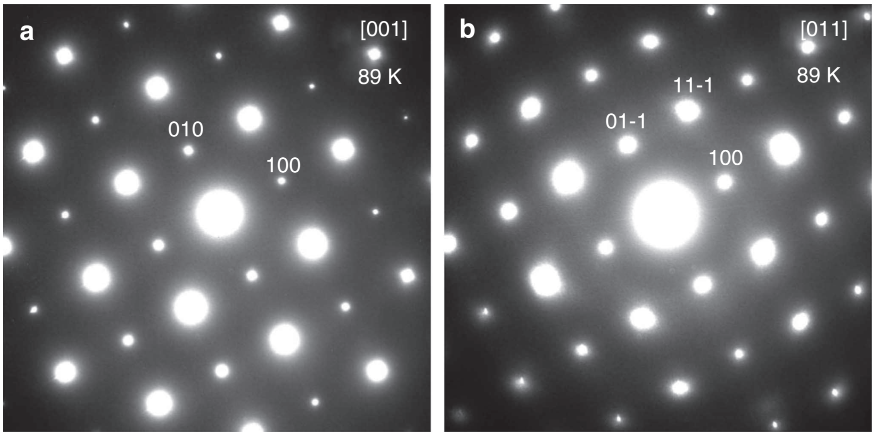

Figure 5 | Electron diffraction patterns of $BaTi_2As_2O$. (**a**) Diffraction pattern with the incident beam along the [001] and (**b**) along the [011] directions. No superlattice peaks are observed at low temperature even after heavy overexposure.

break the rotational symmetry, so can be ruled out. Instead, a simple but novel intra-unit-cell charge order (IUC-CO) naturally explains the observed phenomenology. A transfer of charge from Ti(1) to Ti(2) (see Fig. 1b) lowers the rotational symmetry of the Ti_2O plaquette locally from C_4 to C_2, with the effect on the overall lattice symmetry depending on the ordering pattern of the distinct Ti ions in neighbouring unit cells. Repeating the symmetry-lowered plaquette uniformly along the *a* and *b* directions results in no change of the unit cell, but breaks the metric symmetry from C_4 in *P*4/*mmm* to C_2 in *Pmmm*, as observed experimentally. This arrangement of charges can accordingly be described as a nematic IUC-CO. Our data are therefore consistent with the formation of this type of charge order on cooling through T_a. Such a model is also consistent with the breaking of C_4 symmetry at the *Pn* site that has been observed from $^{121/123}$Sb nuclear resonance measurements[31].

This nematic IUC-CO is energetically favoured on Coulombic grounds if the on-site Hubbard energy *U* is sufficiently small, which is a reasonable assumption as the system is a metal rather than a Mott insulator. The small Hubbard *U* arises from significant screening due to the solvation effect of the high polarizabilities of the As^{3-} and Sb^{3-} anions, which are an order of magnitude larger than that of O^{2-}. Moreover, the As and Sb ions reside on a lower symmetry site in the *Pmmm* structure, which enhances the effects of their polarizabilities. This physics was proposed in an earlier study of the iron-pnictide superconductors[40]. Returning to the present system, the transfer of a charge of δ from Ti(1) to Ti(2) will result in a lowering of the electrostatic energy, $V(1–\delta)(1+\delta)=V(1–\delta^2)$, where V is the screened Coulombic interaction between Ti sites and is positive. The result is charge order with a *d*-wave symmetry[41] with the sign of the modulated charge density varying as $-+-+$ around the plaquette. From plaquette to plaquette, the orientation of the axis of the distortion can be parallel or perpendicular, forming a ferro- or anti-ferro- type ordering, which would preserve or break translational symmetry, respectively. The former is consistent with the experimental observations in this material. We suggest that the rather rigid face-shared octahedral topology in each layer favours the uniform ferro- over the anti-ferro- ordering. It is noteworthy that this *V* is the counterpart of the Coulombic repulsion V_{pp} between neighbouring oxygen atoms in the CuO_2 plane, which was shown to drive IUC nematic order in nonstoichiometric doped cuprates[42]. Hence, the present results obtained on these stoichiometric materials (thus having less ambiguity such as disorder effects) yield insight into the origin of IUC nematic order in the cuprates.

This nematic IUC-CO naturally explains the observed changes in the *a*- and *c*-lattice parameters. The transfer of charge from the Ti(1) $d_{y^2-z^2}$ orbital to Ti(2) $d_{x^2-z^2}$ results in increased electrostatic repulsion between the charge-rich $d_{x^2-z^2}$ orbitals extending along the *a* axis, breaking the tetragonal degeneracy of the *a* and *b* axes and leading to the observed orthorhombic distortion. Furthermore, a uniform stacking of the IUC-CO in each layer can also explain the response of the *c*-lattice parameter, which expands upon entering the charge-ordered state (Fig. 4a). This lattice expansion may be attributed in part to increased electrostatic repulsion between inter-layer Ti ions from the transferred charge. The net energy contribution is $V'[(1+\delta)^2+(1–\delta)^2]=V'(2+2\delta^2)$, where V' is the inter-layer screened Coulombic interaction. This acts in addition to other elastic energy contributions.

The structural effects observed on cooling are much smaller in $BaTi_2Sb_2O$ than $BaTi_2As_2O$, suggesting that the IUC-CO is relatively suppressed both in amplitude and temperature. This may be a result of the larger unit cell in the Sb compound, due to its larger Sb^{3-} ionic diameter (2.25 versus 1.98 Å for As^{3-}; ref. 18), resulting in a smaller *V*.

To identify the microscopic driving force of this nematic instability, we present a symmetry-based zero-order analysis in which only the leading energy scales are retained. Ti atoms reside at the centre of a distorted octahedron with oxygen at the apices and pnictide atoms around the equatorial plane, as shown in Fig. 1d for Ti(1). The Ti 3*d*-energy levels are illustrated in Fig. 1e, similar to the case of nearly isostructural $(LaO)_2CoSe_2O$ (ref. 43). The nominal electron occupation is one electron per Ti atom, which would have been assigned to the locally lowest-lying $d_{y^2-z^2}$ and $d_{x^2-z^2}$ orbitals on the Ti(1) and Ti(2) ions, respectively. However, the σ-bonding between the Ti(1) and Ti(2) d_{xy} orbitals forms a relatively wide band that overlaps the locally lowest level. Therefore, the minimum model for the titanium oxypnictides involves the two orbitals: $d_{y^2-z^2}$ and d_{xy} on Ti(1) and $d_{x^2-z^2}$ and d_{xy} on Ti(2). Since the d_{xy} orbital has the same impact on both the *a* and *b* direction, the C_4–C_2 symmetry lowering around the central oxygen atom is mainly determined by the charge imbalance between the quasi-one-dimensional $d_{y^2-z^2}$ band on Ti(1) and $d_{x^2-z^2}$ on Ti(2) as a result of the Stoner instability[42]. No doubt this mechanism will be complicated by hybridization and other issues, but this symmetry-based analysis provides the appropriate realistic starting point. Since the proposed nematic intra-unit-cell charge order elegantly explains all the observed structural effects, it is anticipated to be the electronic ground state of $BaTi_2Pn_2O$.

Methods

Neutron powder diffraction. Powder specimens of $BaTi_2As_2O$ and $BaTi_2Sb_2O$ were prepared via conventional solid state reaction methods. Details of the synthesis are provided in a previous study[26]. Time-of-flight neutron total scattering experiments were performed at the Neutron Powder Diffractometer at Los Alamos Neutron Science Center (LANSCE) at Los Alamos National Laboratory. Data were collected using a closed-cycle He refrigerator at temperatures ranging from 10–300 K in steps of 10 K near the structural transition and 25 K away from the transition over a wide range of momentum transfer Q. Le Bail[38] fits to the intensity profiles were performed with GSAS[44] on the EXPGUI platform[45]. Pair distribution function (PDF) profiles were obtained by Fourier transforming the measured total scattering intensity up to a maximum momentum transfer of $Q_{\max} = 24\,\text{Å}^{-1}$ using established protocols[46,47] as implemented in the programme PDFgetN[48]. The Le Bail fits were used to extract lattice parameters and space-group symmetry, the PDF fits to extract atomic displacement parameters. Symmetry mode analysis using the programme ISODISTORT[49] was conducted to identify candidate distorted structures.

Electron diffraction and DFT calculations. Electron diffraction patterns were recorded using a JEOL ARM 200CF transmission electron microscope (TEM), operated at 200 keV, at Brookhaven National Laboratory. The TEM samples were prepared by crushing powder specimens into thin flakes transparent to the electron beam, which were supported by a lacey carbon copper grid. DFT calculations were performed within the generalized gradient approximation implemented in the Wien2k software package[50].

References

1. Dagotto, E. *et al. Nanoscale phase Separation and Colossal Magnetoresistance* (Springer-Verlag, 2003).
2. Dagotto, E. Complexity in strongly correlated electronic systems. *Science* **309,** 257–262 (2005).
3. Orenstein, J. & Millis, A. J. Advances in the physics of high-temperature superconductivity. *Science* **288,** 468–474 (2000).
4. da Silva Neto, E. H. *et al.* Ubiquitous interplay between charge ordering and high-temperature superconductivity in cuprates. *Science* **343,** 393–396 (2014).
5. Fernandes, R., Chubukov, A. & Schmalian, J. What drives nematic order in iron-based superconductors? *Nat. Phys.* **10,** 97–104 (2014).
6. Tranquada, J. M., Sternlieb, B. J., Axe, J. D., Nakamura, Y. & Uchida, S. Evidence for stripe correlations of spins and holes in copper oxide superconductors. *Nature* **375,** 561–563 (1995).
7. Hoffman, J. E. *et al.* A four unit cell periodic pattern of quasi-particle states surrounding vortex cores in $Bi_2Sr_2CaCu_2O_{8+\delta}$. *Science* **295,** 466–469 (2002).
8. Vershinin, M. *et al.* Local ordering in the pseudogap state of the high-T_c superconductor $Bi_2Sr_2CaCu_2O_{8+\delta}$. *Science* **303,** 1995–1998 (2004).
9. Chang, J. *et al.* Direct observation of competition between superconductivity and charge density wave order in $YBa_2Cu_3O_{6.67}$. *Nat. Phys.* **8,** 871–876 (2012).
10. Comin, R. *et al.* Charge order driven by Fermi-arc instability in $Bi_2Sr_{2-x}La_xCuO_{6+\delta}$. *Science* **343,** 390–392 (2014).
11. Lawler, M. J. *et al.* Intra-unit-cell nematicity of the high-T_c copper-oxide pseudogap states. *Nature* **466,** 374–377 (2010).
12. Varma, C. Non-Fermi-liquid states and pairing instability of a general model of copper oxide metals. *Phys. Rev. B* **55,** 14554 (1997).
13. Li, Y. *et al.* Hidden magnetic excitation in the pseudogap phase of a high-T_c superconductor. *Nature* **468,** 283–285 (2010).
14. Chuang, T. *et al.* Nematic electronic structure in the 'parent' state of the iron-based superconductor $Ca(Fe_{1-x}Co_x)_2As_2$. *Science* **327,** 181–184 (2010).
15. Lee, P. A., Nagaosa, N. & Wen, X.-G. Doping a mott insulator: Physics of high-temperature superconductivity. *Rev. Mod. Phys.* **78,** 17–85 (2006).
16. Fernandes, R., Chubukov, A., Knolle, J., Eremin, I. & Schmalian, J. Preemptive nematic order, pseudogap, and orbital order in the iron pnictides. *Phys. Rev. B* **85,** 024534 (2012).
17. Yajima, T. *et al.* Synthesis and physical properties of the new oxybismuthides $BaTi_2Bi_2O$ and $(SrF)_2Ti_2Bi_2O$ with a d^1 square net. *J. Phys. Soc. Jpn* **82,** 013703 (2013).
18. Yajima, T. *et al.* Two superconducting phases in the isovalent solid solutions $BaTi_2Pn_2o$ (Pn = As, Sb, and Bi). *J. Phys. Soc. Jpn* **82,** 033705 (2013).
19. Zhai, H.-F. *et al.* Superconductivity, charge- or spin-density wave, and metal-nonmetal transition in $BaTi_2(Sb_{1-x}Bi_x)_2O$. *Phys. Rev. B* **87,** 100502 (2013).
20. Ozawa, T. C. & Kauzlarich, S. M. Chemistry of layered d -metal pnictide oxides and their potential as candidates for new superconductors. *Sci. Technol. Adv. Mater.* **9,** 033003 (2008).
21. Wang, X. F. *et al.* Structure and physical properties for a new layered pnictide-oxide: $BaTi_2As_2O$. *J. Phys: Condens. Mater.* **22,** 075702 (2010).
22. Liu, R. H. *et al.* Structure and physical properties of the layered pnictide-oxides: $(SrF)_2Ti_2Pn_2O$ (Pn = As, Sb) and $(SmO)_2Ti_2Sb_2O$. *Chem. Mater.* **22,** 1503–1508 (2010).
23. Johrendt, D., Hosono, H., Hoffmann, R.-D. & Pöttgen, R. Structural chemistry of superconducting pnictides and pnictide oxides with layered structures. *Z. Kristallogr.* **226,** 435–446 (2011).
24. Yajima, T. *et al.* Superconductivity in $BaTi_2Sb_2O$ with a d^1 square lattice. *J. Phys. Soc. Jpn* **81,** 103706 (2012).
25. Doan, P. *et al.* $Ba_{1-x}Na_xTi_2Sb_2O$ ($0.0 \le x \le 0.33$): a layered titanium-based pnictide oxide superconductor. *J. Am. Chem. Soc.* **134,** 16520–16523 (2012).
26. Nozaki, Y. *et al.* Muon spin relaxation and electron/neutron diffraction studies of $BaTi_2(As_{1-x}Sb_x)_2O$: Absence of static magnetism and superlattice reflections. *Phys. Rev. B* **88,** 214506 (2013).
27. von Rohr, F., Schilling, A., Nesper, R., Baines, C. & Bendele, M. Conventional superconductivity and charge-density-wave ordering in $Ba_{1-x}Na_xTi_2Sb_2O$. *Phys. Rev. B* **88,** 140501 (2013).
28. Gooch, M. *et al.* Weak coupling BCS-like superconductivity in the pnictide oxide $Ba_{1-x}Na_xTi_2Sb_2O$ ($x = 0$ and 0.15). *Phys. Rev. B* **88,** 064510 (2013).
29. Axtell, III E. A., Ozawa, T., Kauzlarich, S. M. & Singh, R. R. Phase transition and spin-gap behavior in a layered tetragonal pnictide oxide. *J. Solid State Chem.* **134,** 423–426 (1997).
30. Liu, R. H. *et al.* Physical properties of the layered pnictide oxides $Na_2Ti_2P_2O$ (P = As,Sb). *Phys. Rev. B* **80,** 144516 (2009).
31. Kitagawa, S., Ishida, K., Nakano, K., Yajima, T. & Kageyama, H. *s*-wave superconductivity in superconducting $BaTi_2Sb_2O$ revealed by $^{121/123}$Sb-NMR/nuclear quadrupole resonance measurements. *Phys. Rev. B* **87,** 060510 (2013).
32. Singh, D. J. Electronic structure, disconnected fermi surfaces and antiferromagnetism in the layered pnictide superconductor $Na_xBa_{1-x}Ti_2Sb_2O$. *New J. Phys.* **14,** 123003 (2012).
33. Wang, G., Zhang, H., Zhang, L. & Liu, C. The electronic structure and magnetism of $BaTi_2Sb_2O$. *J. Appl. Phys.* **113,** 243904 (2013).
34. Subedi, A. Electron-phonon superconductivity and charge density wave instability in the layered titanium-based pnictide $BaTi_2Sb_2O$. *Phys. Rev. B* **87,** 054506 (2013).
35. Xu, H. C. *et al.* Electronic structure of the $BaTi_2As_2O$ parent compound of the titanium-based oxypnictide superconductor. *Phys. Rev. B* **89,** 155108 (2014).
36. Abeykoon, M. *et al.* Evidence for short-range-ordered charge stripes far above the charge-ordering transition in $La_{1.67}Sr_{0.33}NiO_4$. *Phys. Rev. Lett.* **111,** 096404 (2013).
37. Božin, E. S., Billinge, S. J. L., Takagi, H. & Kwei, G. H. Neutron diffraction evidence of microscopic charge inhomogeneities in the CuO_2 plane of superconducting $La_{2-x}Sr_xCu_4$ ($0 \le x \le 0.30$). *Phys. Rev. Lett.* **84,** 5856–5859 (2000).
38. Le Bail, A., Duroy, H. & Fourquet, J. L. *Ab-initio* structure determination of $LiSbWO_6$ by X-ray powder diffraction. *Mater. Res. Bull.* **23,** 447–452 (1987).
39. Fujita, K. *et al.* Direct phase-sensitive identification of a *d*-form factor density wave in underdoped cuprates. *Proc. Natl Acad. Sci. USA* **111,** E3026–E3032 (2014).
40. Sawatzky, G., Elfimov, I., van den Brink, J. & Zaanen, J. Heavy-anion solvation of polarity fluctuations in pnictides. *Europhys. Lett.* **86,** 17006 (2009).
41. Fradkin, E., Kivelson, S. A., Lawler, M. J., Eisenstein, J. P. & Mackenzie, A. P. Nematic fermi fluids in condensed matter physics. *Annu. Rev. Condens. Matter Phys.* **1,** 153 (2010).
42. Fischer, M. H. & Kim, E.-A. Mean-field analysis of intra-unit-cell order in the Emery model of the CuO_2 plane. *Phys. Rev. B* **84,** 144502 (2011).
43. Wu, H. Electronic structure, spin state, and magnetism of the square-lattice mott insulator $LaCo_2Se_2O_3$ from first principles. *Phys. Rev. B* **82,** 020410(R) (2010).
44. Larson, A. C. & Von Dreele, R. B. *General structure Analysis System*. Report No. LAUR-86-748, 87545 (Los Alamos National Laboratory, 1994).
45. Toby, B. H. EXPGUI, a graphical user interface for GSAS. *J. Appl. Crystallogr.* **34,** 201–213 (2001).
46. Egami, T. & Billinge, S. J. L. *Underneath the Bragg Peaks: Structural Analysis of Complex Materials* 2nd edn (Elsevier, 2012).
47. Chupas, P. J. *et al.* Rapid acquisition pair distribution function analysis (RA-PDF). *J. Appl. Crystallogr.* **36,** 1342–1347 (2003).
48. Peterson, P. F., Gutmann, M., Proffen, T. & Billinge, S. J. L. PDFgetN: a user-friendly program to extract the total scattering structure function and the pair distribution function from neutron powder diffraction data. *J. Appl. Crystallogr.* **33,** 1192–1192 (2000).
49. Campbell, B., Stokes, H., Tanner, D. & Hatch, D. ISODISPLACE: an internet tool for exploring structural distortions. *J. Appl. Crystallogr.* **39,** 607–614 (2006).
50. Blaha, P., Schwarz, K., Madsen, G., Kvasnicka, D. & Luitz, J. *WIEN2k: An Augmented Plane Wave Plus Local Orbitals Program for Calculating Crystal Properties* (Vienna University Technology, 2001).

Acknowledgements

Work at Brookhaven National Laboratory was supported by the U.S. Department of Energy, Office of Basic Energy Sciences, under contract No. DE-AC02-98CH10886.

Work at Columbia University was supported by the U.S. National Science Foundation (NSF) Partnership for International Research and Education (PIRE) Super-PIRE project (grant OISE-0968226). Y.J.U. also acknowledges support from NSF DMR-1105961, the Japan Atomic Energy Agency Reimei project, and the Friends of Todai Inc. The work at Kyoto University was supported by the FIRST program, Japan Society of the Promotion of Science (JSPS). Neutron scattering experiments were carried out on NPDF at LANSCE, funded by DOE Office of Basic Energy Sciences. LANL is operated by Los Alamos National Security LLC under DOE Contract No. DE-AC52-06NA25396.

Author contributions

Y.J.U., S.J.L.B. and B.A.F. initiated this work. Y.N. and H.K. carried out sample preparation and characterization. E.S.B. carried out the neutron diffraction measurements and analysed the data with assistance from B.A.F. H.H. performed the electron diffraction measurements with help from Y.Z. W.-G.Y. proposed the charge-ordering model and provided theoretical support. B.A.F., W.-G.Y. and S.J.L.B. wrote the paper, with input from all the authors.

Additional information

Supplementary Information accompanies this paper at http://www.nature.com/naturecommunications

Competing financial interests: The authors declare no competing financial interests.

How to cite this article: Frandsen, B. A. *et al.* Intra-unit-cell nematic charge order in the titanium-oxypnictide family of superconductors. *Nat. Commun.* 5:5761 doi: 10.1038/ncomms6761 (2014).